

EFFECTS OF UNIFORM AND DIFFERENTIAL ROTATION ON STELLAR PULSATIONS

C. C. LOVEKIN^{1,3}, R. G. DEUPREE¹, AND M. J. CLEMENT²

¹ Institute for Computational Astrophysics, Department of Astronomy and Physics, Saint Mary's University, Halifax, NS B3H 3C3, Canada; clovekin@ap.smu.ca

² Department of Astronomy and Astrophysics, University of Toronto, Toronto, ON M5S 3H8, Canada

Received 2008 June 18; accepted 2008 November 12; published 2009 March 2

ABSTRACT

We have investigated the effects of uniform rotation and a specific model for differential rotation on the pulsation frequencies of $10 M_{\odot}$ stellar models. Uniform rotation decreases the frequencies for all modes. Differential rotation does not appear to have a significant effect on the frequencies, except for the most extreme differentially rotating models. In all cases, the large and small separations show the effects of rotation at lower velocities than do the individual frequencies. Unfortunately, to a certain extent, differential rotation mimics the effects of more rapid rotation, and only the presence of some specific observed frequencies with well identified modes will be able to uniquely constrain the internal rotation of pulsating stars.

Key words: stars: oscillations – stars: rotation

1. INTRODUCTION

Observationally detected stellar pulsation frequencies can be used to place constraints on stellar models, giving us an improved understanding of the interior structure and evolution of stars. The most successful application has been the Sun, where the large number of observed modes have placed strict constraints on parameters such as the helium abundance (Y) (Basu & Antia 2004; Antia & Basu 2006), the depth of the convection zone (Christensen-Dalsgaard et al. 1989, 1991), and the interior angular momentum distribution (Eff-Darwich et al. 2002; Couvidat et al. 2003). Observations of pulsation frequencies of other stars continue to improve, particularly through dedicated satellites such as *WIRE* (Hacking et al. 1999), *MOST* (Walker et al. 2003), *CoRoT* (Baglin et al. 2001), and *Kepler* (Basri et al. 2005), as well as ground-based networks such as STEPHI (Belmonte et al. 1993) and WET (Nather et al. 1990). These improved observations, giving us long-term coverage and improved accuracy, are the first steps in enabling other stars to be constrained in a similar manner to the Sun. Asteroseismology, then, has the potential to answer a number of questions about the interior structure of stars throughout the HR diagram. One aspect of stellar structure which could be explored using asteroseismology is the internal rotation rate. It is theoretically possible for stars to rotate with angular velocity increasing or decreasing with distance from the rotation axis, and there is some evidence that the latter may be true in massive main-sequence stars, at least at the surface (Stoeckley 1968). A third possibility is uniform rotation. It has been argued that uniform rotation is unrealistic based on observations of the Praesepe and Hyades clusters (Smith 1971). Of course, other, less well structured rotation laws are possible. However, there is little evidence in support of a specific rotation law, and the large uncertainties prevent any of the possibilities from being ruled out. We note in passing that the solar rotation rate in the convection zone is primarily dependent on latitude (Schou et al. 1998; Thompson et al. 2003) and thus cannot be described by a conservative rotation law.

Recently, interferometric observations of Achernar (Domiciano de Souza et al. 2003) found that this star is far

more oblate than is possible for a uniformly rotating star. This is true because uniformly rotating stars reach critical rotation before they have sufficient angular momentum to produce such an oblate object. However, Jackson et al. (2005) noted that models in which the rotation rate increases inward from the surface can produce the oblateness observed for Achernar and still match the observed $v \sin i$. While further study has proposed that the oblateness may be due to a circumstellar envelope (Carcofi et al. 2008), the original conclusion does raise the interesting question as to whether stars with rotation laws required to produce such an oblate shape exist and, if so, whether these rotation laws could be identified by possible pulsation modes. We investigate this possibility in this paper.

Differential rotation with the rotation rate increasing inward, as is considered in this paper, will have an impact on the deep interior structure of the star, provided the differential rotation is large enough. Rapid rotation in the outer layers of a star has little to no effect on the gravitational potential and core structure, as the envelope contains a relatively small fraction of the stellar mass. In fact, many early attempts to model rotating stars assumed that the mass in the envelope was negligible and that the gravitational potential in this region could be modeled using a Roche potential (Sackmann & Anand 1970). However, it was recognized early on that this assumption was not always valid. Efforts to model a wider variety of rotating stars were made through the implementation of the self-consistent field (SCF) method (Ostriker & Mark 1968), or through direct, 2D finite difference solutions to Poisson's equation (Clement 1974, 1978, 1979). These methods allowed stars to be modeled with differential rotation, at least under certain circumstances. Concentrating angular momentum in the center, unlike uniform rotation, can produce enough distortion to affect the core, and consequently the evolution of the star. Only in this case can we produce a model with interior properties significantly different from the uniformly rotating model (Sackmann & Anand 1970). Even restricting ourselves to this type of differential rotation does not narrow the possibilities significantly. The rotation could be shellular, as proposed by Zahn (1992), or cylindrical (conservative rotation laws). In this paper, we have focused on conservative rotation laws, either with uniform rotation or with the rotation rate increasing toward the center of the star. Further discussion of our models can be found in Section 2. In Section 3

³ Current address: Observatoire de Paris, LESIA, CNRS UMR 8109, F-92195 Meudon, France.

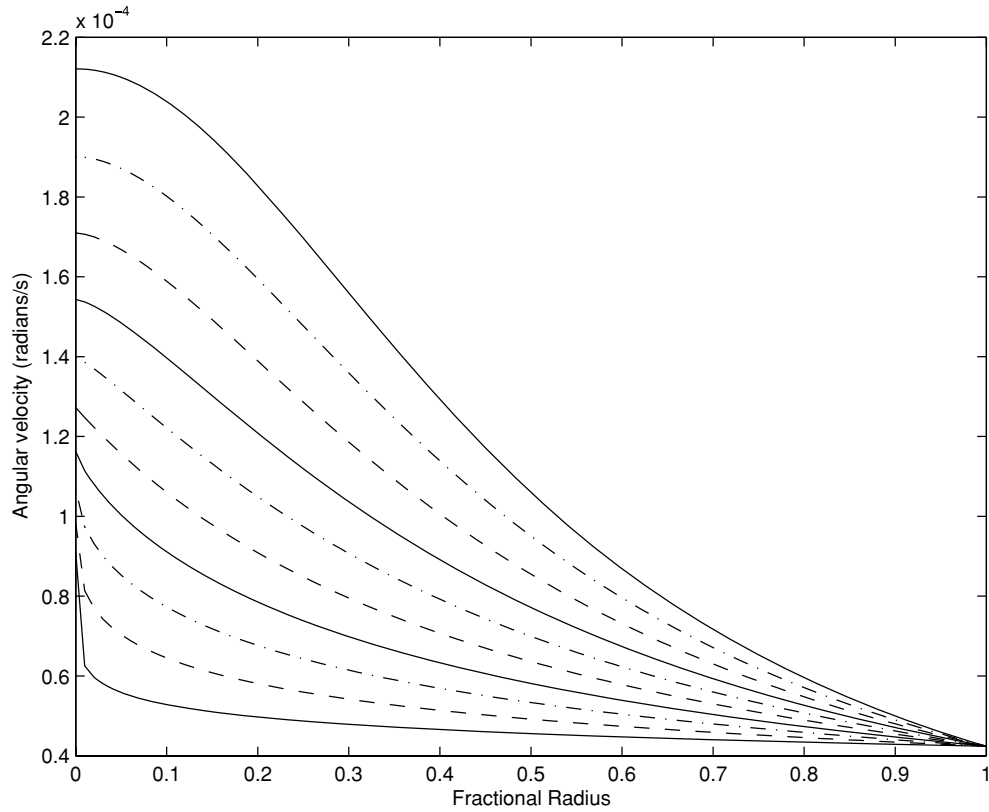


Figure 1. Rotation law used in differentially rotating models (Equation (2)). Curves show from bottom to top the rotation law for $\beta = 0.2, 0.4, 0.6, 0.8, 1.0, 1.2, 1.4, 1.6, 1.8,$ and 2.0 for a model with a surface equatorial velocity of 120 km s^{-1} .

we consider the eigenfrequencies of rotating models as well as the large and small separations in Sections 4 and 5, respectively. Our conclusions are summarized in Section 6.

2. NUMERICAL MODELS

The stellar models are computed using the 2D stellar structure code ROTORC (Deupree 1990, 1995). The code uses the OPAL opacities (Iglesias & Rogers 1996) and equation of state (Rogers et al. 1996). Here we consider only $10 M_{\odot}$ ZAMS models with $X = 0.7, Z = 0.02$. These models solve the conservation equations of mass, momentum, energy, and hydrogen abundance along with Poisson’s equation for the gravitational potential on a two-dimensional finite difference grid with the fractional surface equatorial radius and the colatitude as the independent variables. The surface equatorial radius is determined by requiring that the integral of the density over the volume of the model equals the stellar mass. The ZAMS models are taken to be time independent and static, except for the imposed rotation law, so that the mass, azimuthal momentum, and hydrogen composition conservation equations drop out.

The only change required in the stellar evolution code for nonuniform cylindrical rotation laws is the addition of an extra term in the total potential (e.g., Tassoul 2000):

$$\begin{aligned} \Psi &= \Phi - \int_0^{\varpi} \Omega^2(\varpi') \varpi' d\varpi' \\ &= \Phi - \frac{\Omega^2 \varpi^2}{2} + \int_0^{\varpi} \varpi'^2 \Omega(\varpi') \frac{d\Omega(\varpi')}{d\varpi'} d\varpi' \end{aligned} \quad (1)$$

where Ω is the rotation velocity (in radians per second) and ϖ is the distance from the rotation axis ($x \sin \theta$, where x is the

fractional surface equatorial radius and θ is the colatitude). The extra term is the last term on the right-hand side of the equation. Performing the integral is straightforward for an analytically imposed rotation rate distribution in the ZAMS models. The total potential is used only to determine the surface location at each latitude by taking the surface to be an equipotential. Although defining a total potential requires a conservative rotation law, this is the only way in which a conservative rotation law is utilized in the stellar structure code.

We have constructed uniformly rotating ZAMS models with rotation velocities between 0 and 360 km s^{-1} , with an approximate spacing of 30 km s^{-1} . We have also computed a number of differentially rotating models at two values of the surface equatorial rotation velocity, 120 and 240 km s^{-1} . The differential rotation law is as given by Jackson et al. (2005):

$$\Omega(\varpi) = \frac{\Omega_o}{1 + (a\varpi)^\beta} \quad (2)$$

where β is a parameter ranging from 0 (uniform rotation) to 2, the maximum allowed for stability. The parameters a and Ω_o are used to impose the desired surface equatorial velocity and shape of the rotation law at small distances from the rotation axis. We have arbitrarily chosen $a = 2$. Figure 1 shows the rotation rate as a function of distance perpendicular to the rotation axis for a surface equatorial rotation velocity of 120 km s^{-1} and a surface equatorial radius for a uniformly rotating model at that speed. Increasing β increases the rotation rate close to the rotation axis, including in the core of the star. Increasing angular momentum increases structural changes, and thus the structural changes increase with increasing β . It is expected that increasing the rotation rate through increasing β may, in some ways, mimic more rapid uniform rotation.

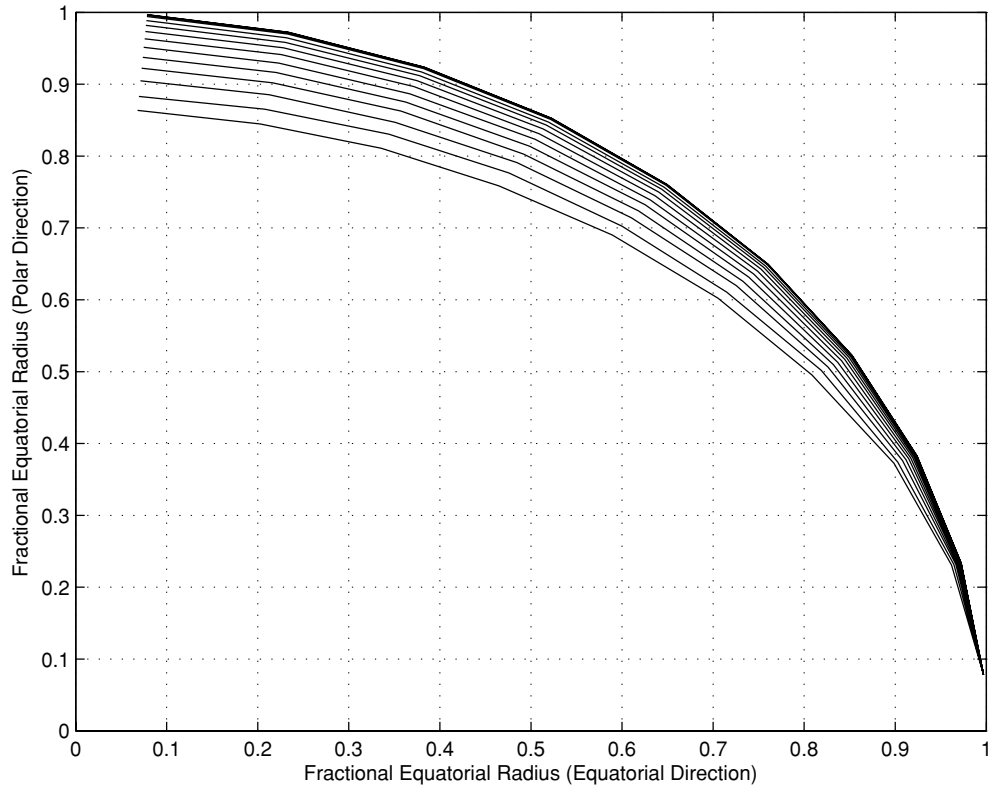


Figure 2. Surface shape for uniformly rotating models. The polar radius decreases relative to the equatorial radius as rotation increases from 0 km s⁻¹ to 360 km s⁻¹.

One major result produced by significant rotation is an appreciable distortion of the surface of the model. We present the surface shape for a set of uniformly rotating models with surface equatorial velocities ranging from 0 to 360 km s⁻¹ in Figure 2. For each model the equatorial radius is taken to be unity. The ratio between the polar and equatorial radius decreases with increasing rotation, as the polar radius decreases slightly while the equatorial radius increases considerably. Differential rotation in which the rotation rate increases with decreasing distance from the rotation axis amplifies this effect. We present the surface shape for the differentially rotating models in Figure 3. The solid curves are for a surface equatorial velocity of 120 km s⁻¹, while the dashed curves denote a surface equatorial velocity of 240 km s⁻¹. As the parameter β in Equation (2) increases, the fractional polar radius decreases. The change in fractional radius with β is greatest at the pole and decreases toward the equator. Note that the fractional polar radius for a model rotating with a surface equatorial velocity of 120 km s⁻¹ and a value of β of 1.8 has nearly the same fractional polar radius as a model uniformly rotating at 240 km s⁻¹.

We have increased the radial resolution of the static models by more than a factor of 2 over that used by Lovekin and Deupree (2008). The intent is to reduce the scatter and uncertainty in the pulsation mode calculations, particularly for the large and small separations. By and large this has been successful.

The determination of the pulsational properties of these models is made using the linear adiabatic pulsation code developed by Clement (1998). We restrict our attention to input models with conservative rotation laws so that we can write the effective gravity (\vec{g}) as the derivative of the total potential. The input models are axisymmetric spheroids, which allows us to assume a $e^{i[\omega t + m\phi]}$ time and azimuthal dependence. The equations to be linearized are the three components of

the momentum conservation equation, the mass conservation equation, the adiabatic relation between the density (ρ) and the pressure (P), and Poisson’s equation. The dependent variables are the three components of the linearized displacements ($\vec{\xi}$), the linearized Eulerian displacements of the density ($\delta\rho$), pressure (δP), and the gravitational potential ($\delta\phi$). We start with the perturbed momentum equation:

$$\delta \left(\frac{d\vec{v}}{dt} \right) = \delta \left(\frac{\partial \vec{v}}{\partial t} + [\vec{v} \cdot \nabla] \vec{v} \right) = \nabla(\delta\phi) + \left(\frac{\delta\rho}{\rho^2} \right) \nabla P - \frac{1}{\rho} \nabla \delta P \quad (3)$$

where \vec{v} is the velocity, which includes both the pulsational perturbations and the velocity distribution of the unperturbed model. Here we assume this latter velocity results exclusively from rotation, and is given by

$$\vec{v} = v\hat{\phi} = \Omega r \sin(\theta)\hat{\phi}. \quad (4)$$

Here Ω is the rotation rate, and our assumption of a conservative rotation law requires it to be a function only of the distance from the rotation axis, $\varpi = r \sin(\theta)$. We can write an expression for the Eulerian perturbation of the velocity in terms of the displacements because the Lagrangian time derivative of the displacement is the Lagrangian velocity perturbation. Thus,

$$\delta \vec{v} = \frac{\partial \vec{\xi}}{\partial t} + (\vec{v} \cdot \nabla) \vec{\xi} - (\vec{\xi} \cdot \nabla) \vec{v}. \quad (5)$$

Substituting this expression into the above perturbed momentum equation and proceeding along the same lines as Clement (1998) leads to the following expressions for the three individual

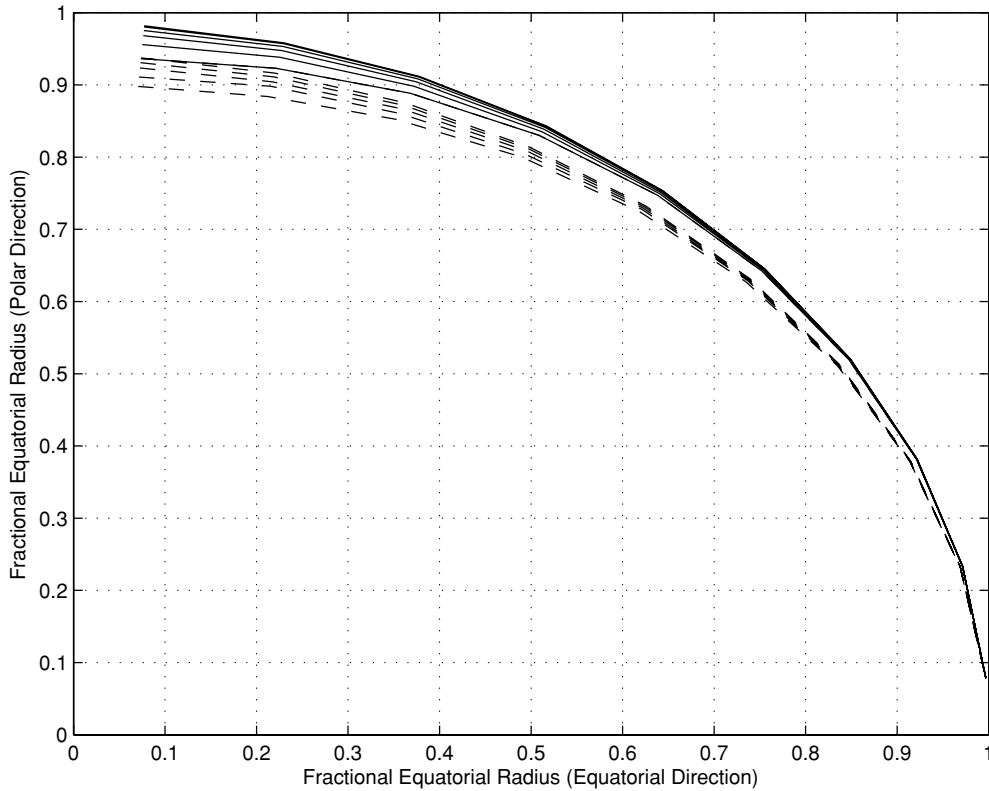


Figure 3. Surface shape for differentially rotating models at 120 km s^{-1} (solid) and 240 km s^{-1} (dashed). As the rotation rate close to the rotation axis increases (increasing β), the polar radius decreases relative to the uniformly rotating case.

components of the momentum equation:

$$\begin{aligned} \sigma^2 \xi_r + 2i\sigma\Omega\xi_\phi \sin\theta - \varpi \sin\theta \left[\xi_r \frac{\partial\Omega^2}{\partial r} + \frac{\xi_\theta}{r} \frac{\partial\Omega^2}{\partial\theta} \right] - \frac{\partial\delta p}{\partial r} \\ = -Ag_r(\nabla \cdot \vec{\xi}) \end{aligned} \quad (6)$$

$$\begin{aligned} \sigma^2 \xi_\theta + 2i\sigma\Omega\xi_\phi \cos\theta - \varpi \cos\theta \left[\xi_r \frac{\partial\Omega^2}{\partial r} + \frac{\xi_\theta}{r} \frac{\partial\Omega^2}{\partial\theta} \right] - \frac{1}{r} \frac{\partial\delta p}{\partial\theta} \\ = -Ag_\theta(\nabla \cdot \vec{\xi}) \end{aligned} \quad (7)$$

$$\sigma^2 \xi_\phi - 2i\sigma\Omega(\xi_r \sin\theta + \xi_\theta \cos\theta) - \frac{im}{r \sin\theta} \delta p = 0, \quad (8)$$

where $\sigma = \omega + m\Omega$, $\delta p = \delta P/\rho - \delta\phi$, $A = c^2 d \ln \rho / d\Psi - 1$, and $c^2 = \Gamma_1 P/\rho$. The quantity c is the adiabatic sound speed. The other equations required are as listed in Clement (1998): mass conservation, the adiabatic relationship between the density and pressure perturbations, and Poisson's equation for the perturbed gravitational potential:

$$\delta\rho = -\nabla \cdot \rho \vec{\xi} \quad (9)$$

$$\delta P = -\Gamma_1 P \nabla \cdot \vec{\xi} - \xi \cdot \nabla P \quad (10)$$

$$\nabla^2 \delta\phi = -4\pi G \delta\rho. \quad (11)$$

Differential rotation has introduced two new terms into each of the radial and latitudinal momentum equations. The other change is that σ , the eigenfrequency in the local rotating frame, is no longer constant except for axisymmetric modes. This does not alter the solution algorithm, however, because Clement's (1998) approach was to select σ (which now becomes selecting ω and calculating σ locally as needed), solve all the equations, and see if a discriminant was satisfied. Neither the added terms nor the nature of the eigenvalue requires any further

modification to the approach, and the derivation of the final equations proceeds as described by Clement (1998).

Using these equations we can calculate the pulsation properties of the stellar models on a 2D finite difference grid. This is done through a change of variables, factoring out the behavior of ξ_r , ξ_θ , δp and $\delta\phi$ near the boundaries to eliminate singularities. The coefficients of these equations can be put in a band-diagonal matrix and solved. NRO can include up to nine angular zones in the eigenfunction solution. This gives the solution at N angles, where N is the number of angular zones, which can subsequently be decomposed into the contributions of individual spherical harmonics through the use of Fourier transforms. Throughout this paper, we have used $N = 6$. Based on the calculations of Lovekin & Deupree (2008), six spherical harmonics are sufficient to accurately calculate the eigenfrequencies for the most rapidly rotating models discussed here. Indeed, we have performed a few test calculations with $N = 8$ and have found that the effect on the frequencies is small, typically a few hundredths of a percent.

As discussed in Lovekin & Deupree (2008), NRO, combined with stellar structure models from ROTORC, allows us to calculate the pulsation frequencies for rotating stars without making any a priori assumptions about the structure, except that the rotation law is conservative for NRO. For further discussion of the method of solution used by NRO, see Clement (1998) or Lovekin & Deupree (2008).

With spherical stellar models, the radial and angular components of the perturbations separate, and the angular part can be expressed as a spherical harmonic with specific values of the quantum numbers l and m .

For rotating stars, the eigenfunction solution is not a single spherical harmonic, and l is not a valid quantum number. Indeed, NRO uses l only to specify the parity of the mode being calculated,

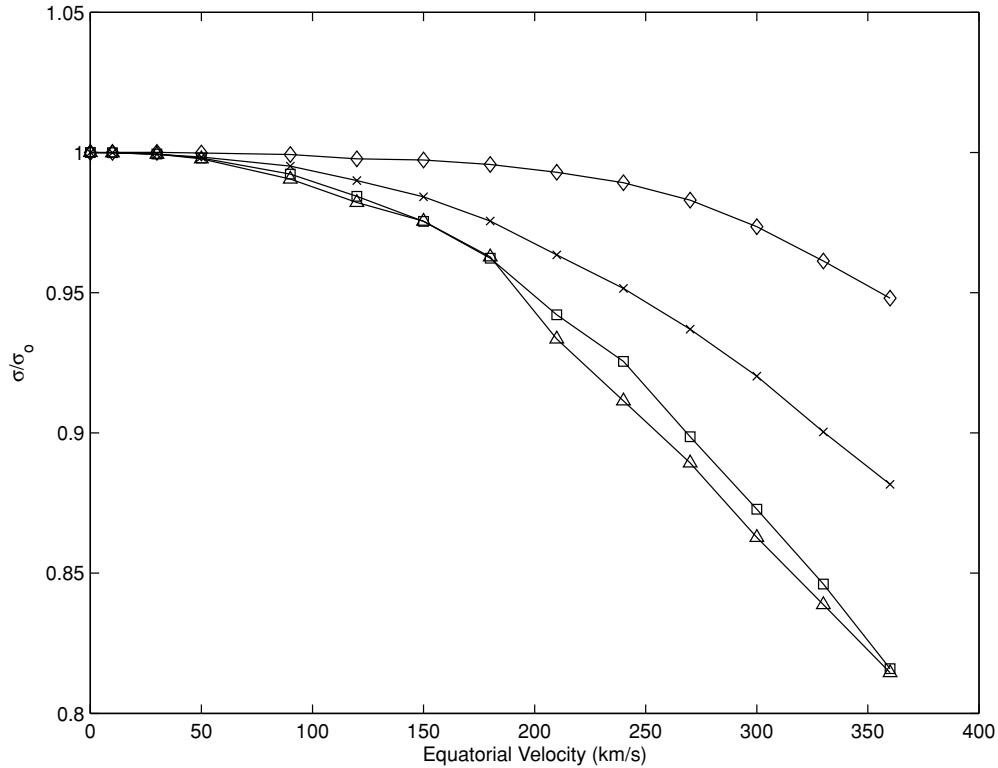


Figure 4. First four harmonics of the $l_o = 2$ mode for a uniformly rotating $10 M_\odot$ model as a function of the rotation rate. The four curves represent the frequencies for the f (diamond), p_1 (\times), p_2 (square), and p_3 (triangle) modes.

and includes the first k even or odd spherical harmonics, where k is the number of angles included. We identify modes using a quantum number l_o , which is the l of the mode in the nonrotating model to which a given mode can be traced. For spheroids, m remains a valid quantum number. As in Lovekin & Deupree (2008), we restrict ourselves to axisymmetric modes ($m = 0$) and modes with small radial quantum number (n).

3. RELATIVE FREQUENCIES

In this paper, we consider low-order axisymmetric modes for $l_o = 0, 1, 2$, and 3. These modes are expected to have the highest amplitudes and the smallest cancellation effects across the visible surface of the star, and are hence expected to be the most easily visible. Our structural models cover velocities from 0 to 360 km s^{-1} and for two velocities, 120 and 240 km s^{-1} , we have calculated differentially rotating models with β varying from 0 to 2.0. Tracing the individual modes becomes very difficult above rotation velocities of 360 km s^{-1} and for some higher values of β , and this represents a practical limit to our study. Although the frequencies can be calculated at these velocities, the resulting eigenfunctions are a mix of six spherical harmonics, and no single harmonic dominates. As it is very difficult to reliably assign a value of l_o to these modes, we exclude them from our analysis. It is probably feasible to trace the modes accurately, but this could require an extremely fine rotational velocity grid ($1\text{--}5 \text{ km s}^{-1}$). We decided not to pursue this for this exploratory work. For differentially rotating models, the limits are $\beta = 1.8$ for the 120 km s^{-1} model and $\beta = 1.0$ for the 240 km s^{-1} model. Based on the curves shown in Figure 1, it appears that the limit is related to the angular velocity near the rotation axis. The curve representing $\beta = 1.0$ has approximately half the value at the center of the $\beta = 2.0$ curve. Therefore, if we double the velocities everywhere, the

limiting β should move from 1.8 at 120 km s^{-1} to 1.0 at 240 km s^{-1} , which corresponds to approximately the same angular velocity near the rotation axis.

3.1. Uniform Rotation

The trends produced by tracing a given mode through increases in rotation velocity are illustrated in Figure 4 for the $l_o = 2$ mode, which shows the eigenfrequencies normalized by the nonrotating frequency for each mode. Overall, the trends we find for frequency agree with those calculated by previous work (Lignières et al. 2006). These authors find that the frequencies decrease as one increases the rotation rate, with higher frequency modes decreasing more than lower modes. As discussed in Lovekin & Deupree (2008), our results at low to moderate rotation rates are also consistent with the frequency trends predicted by second-order perturbation theory (see, for example, Saio 1981).

We have increased the radial resolution of the outer 30% of the radius of the static models by more than a factor of 2 over that used by Lovekin & Deupree (2008). This produces a radial zoning finer than that currently allowed by the pulsation code, so further increases in radial resolution in the 2D structure models will only be effective if the pulsation code is modified to allow more radial zones. The intent of the modified zoning is to reduce the scatter and uncertainty in the mode calculations evident in Lovekin & Deupree (2008). Figure 4 shows that a reasonable estimate of our accuracy for the frequencies is a very few tenths of a percent, although there are still a few frequencies, most commonly but not exclusively for the higher radial orders and higher rotation rates, which do not fit within this limit. One might expect the radial resolution near the rotation axis and at mid latitudes to be less than for lower rotation rates because the fractional radius at these latitudes compared to the equator

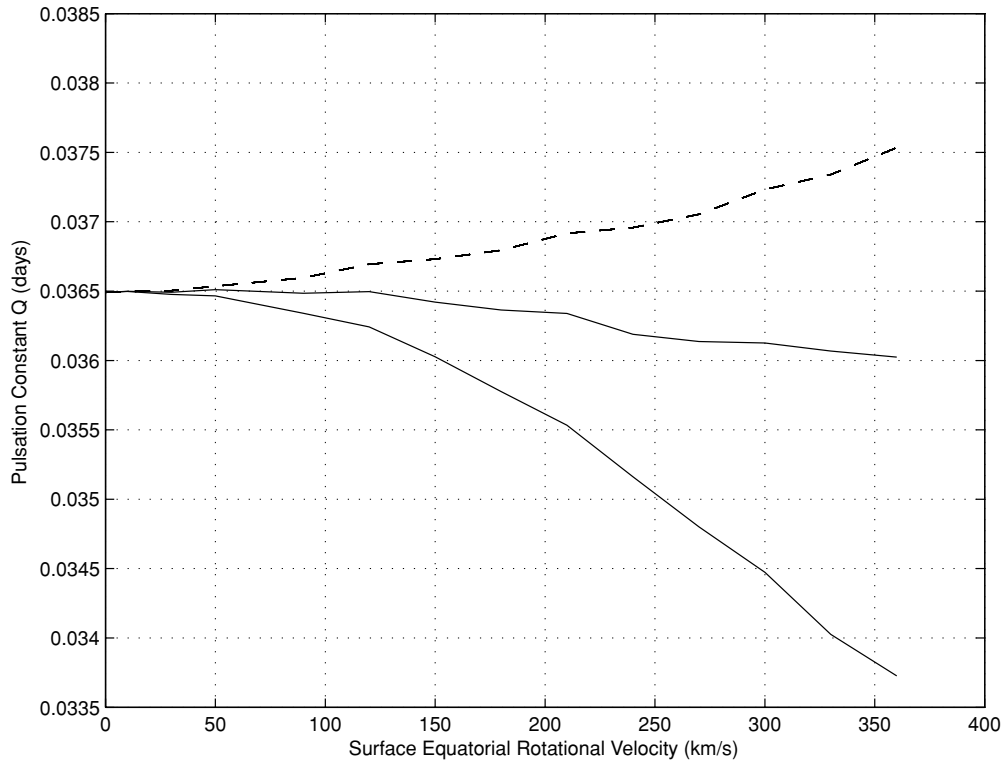


Figure 5. Plot of the pulsation constant for the radius of a sphere with the same volume as the rotating model (bottom) and the radius at colatitude of 40° (middle). Also shown is the pulsation constant assuming there is no change to the mean density as the rotation rate increases (dashed curve).

is lower. The accuracy of the small separation appears well within a μHz , while the large separation does show variations on the order of one μHz , particularly at higher rotation velocities and for higher radial order modes. This is compatible with the notion that the radial resolution near the surface could continue to benefit from refinement. However, these uncertainties do not disguise trends in the results, even in the large separation, with respect to rotation rate or the rotation law, and we consider these trends significant.

One interesting line of inquiry is whether there is some analog to the period–mean density relation which allows interpolation of eigenfrequencies as functions of models and rotation rates. Specifically, we have examined if there is a physically meaningful radius which can be used in the period–mean density relation

$$Q = P \sqrt{\frac{M}{R^3}} \quad (12)$$

(where M and R are in solar units, and P is the period) that would allow Q to be approximately constant as a function of the rotation rate. The comparatively small changes in the eigenfrequencies shown in Figure 4 suggest that the surface equatorial radius, with its fairly rapid increase as a function of rotation, will not keep Q approximately constant, and it does not. The same is true for an average radius, defined as either a straight average or the effective radius required to contain the total volume of the model. The polar radius would be more promising because it only slowly varies with the rotation rate, but it actually decreases slightly as the rotation rate increases. This is the wrong direction to keep Q constant because the frequency decreases as well. Because the polar radius decreases slightly and the equatorial radius increases appreciably with increasing rotation, one might guess there would be some latitude at which the radius increases at a rate that nearly offsets the rate of period increase. This is

true, and occurs at a colatitude of 40° . It is not obvious that this has any physical significance because it is difficult to associate any specific meaning to the radius at this latitude. We present the pulsation constant for two definitions of an effective radius in Figure 5. One way is to use the radius of a sphere with the same volume as the model. The other uses the radius at a colatitude of 40° . For comparison we show a “pulsation constant” that would exist if we used the mean density of the nonrotating model. We include this to give an idea of the size of the effect. Interestingly, the variation in the pulsation constant is significantly larger, allowing the mean density to be determined by the total volume of the rotating model (the mass is the same for all models), than it is when the mean density is assumed to be that of the nonrotating model.

The frequencies can also be changed by the mass or evolutionary state of the star, producing trends that could potentially be confused with rotational effects. We wish to determine how closely the frequencies of a rotating model can be mimicked by a nonrotating model. First we calculated the Q values for each model in the 10 and 12 M_\odot nonrotating models. For each mode, we then took the mean of the Q of the two models. We used this average Q for the radial fundamental mode and the frequency of the radial fundamental mode for the model rotating at 150 km s^{-1} to calculate a mean density. This corresponds to the mean density of a nonrotating model of unknown mass and radius pulsating in the radial fundamental mode with the same frequency as the 10 M_\odot model rotating at 150 km s^{-1} . The mean density found this way and the average Q ’s for the other l_o ’s can be used to predict the other frequencies of this presumed non-rotating model. When these frequencies are compared to the calculated frequencies for the rotating model, the differences are significant. Using Q to calculate the frequencies in this way forces the radial fundamental mode to have the same frequency, so the differences between frequencies should be solely a result of

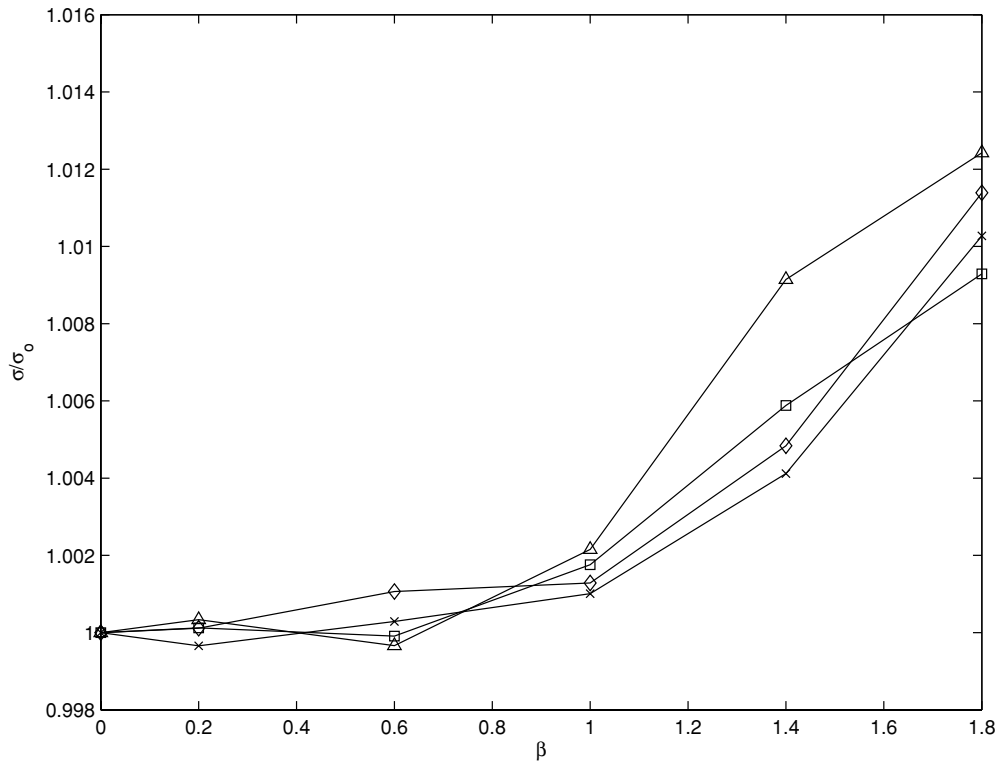


Figure 6. The fundamental and first three overtones of the $l_o = 0$ mode for a model rotating at 120 km s^{-1} as a function of the differential rotation parameter β (see Equation (2)). The four curves represent the frequencies for the fundamental (diamond), 1H (\times), 2H (square), and 3H (triangle) modes.

rotation. The frequencies predicted for the $l_o = 0$ and 2 modes are larger by 1–5%, with the differences increasing for higher order modes. At the same time, the frequencies predicted for the $l_o = 1$ and 3 modes are smaller, by as much as 15% for the $l_o = 1 p_1$ mode. As the radial order increases, the differences between the rotating model and the nonrotating calculation decrease for the $l_o = 1$ modes, but increase for the $l_o = 3$ modes. The size and direction of these trends imply that the pulsation spectrum of a rotating model is unlikely to be confused with the pulsation spectrum of a more massive nonrotating model. It also suggests that rotation must be included in the calculations if observations indicate it might be present even at this moderate amount.

We have also evolved a single nonrotating model, and compared the ZAMS model with one part way through the main-sequence evolution ($X_c = 0.47$). In this case, the frequencies decreased sufficiently, even for a model with a large remaining core hydrogen fraction, that confusion seems unlikely.

3.2. Differential Rotation

We have studied the change in the frequencies of $10 M_\odot$ ZAMS models differentially rotating at 120 km s^{-1} and 240 km s^{-1} . Overall, the frequencies increase for $l_o = 0$ and 1, and decrease for $l_o = 2$ and 3, a trend seen at both 120 km s^{-1} and 240 km s^{-1} . Our results for $l_o = 0$ are shown in Figure 6 for the fundamental, 1H, 2H, and 3H modes for a model rotating at 120 km s^{-1} . In this case, the frequency changes are largest for the 3H modes, but are noticeable for all modes by $\beta \approx 1$. Similar trends are found for the other values of l_o considered here. Still, the differences remain relatively small, and it seems unlikely that even extreme differential rotation with this surface rotation velocity will be detectable using the values of the eigenfrequencies alone.

The frequency results for the 240 km s^{-1} model, shown in Figure 7 for $l_o = 0$, are slightly more promising. Although we were unable to reliably identify modes above $\beta = 1.0$, the frequencies already differ by more than 1% by $\beta = 1.0$ for the 1H mode, and it seems the differences would be noticeable by $\beta = 0.4$. If this trend continues, as seems likely at least for the F and 1H modes, the frequency differences should be large enough to be detectable in these more rapidly rotating stars. As noted above, for some modes differential rotation causes the frequencies to increase as in Figures 7 and 8, while for others the frequencies decrease, as in Figure 9. These plots do not include the 3H mode, as we found that the scatter in this mode remained a significant fraction of the variation, despite the improved radial zoning, and so have chosen not to include it in our discussion.

The effects of differential rotation compared with uniform rotation are shown in Figure 9 for the $l_o = 2 p_2$ mode. Differential rotation can change the frequencies by about a percent above and beyond the difference predicted based on surface equatorial velocity alone. The differences are small, about 1% for the most extreme differentially rotating model at 120 km s^{-1} . Based on the frequencies we have calculated, it may be possible to discriminate between uniform and this type of differential rotation, given the right combination of properly identified frequencies. Since frequencies increase relative to the uniformly rotating case for some l_o and decrease for others, these differences could be used to constrain the rotation. This would require a star with a few positively identified modes, some of which were either $l_o = 0$ or 1, and some of which were either $l_o = 2$ or 3. The number of modes required and the challenges presented by accurate mode identification in massive main-sequence stars may make this extremely difficult in practice.

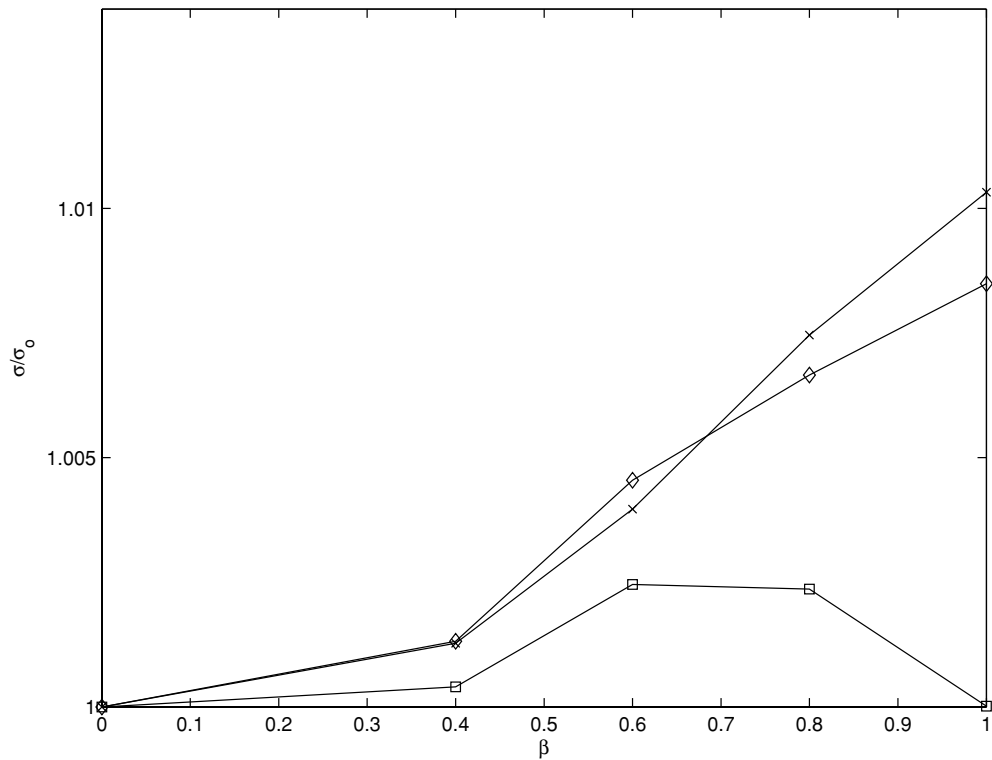


Figure 7. Relative frequencies of the $l_o = 0$ modes versus differential rotation parameter β for a model rotating at 240 km s^{-1} . The curves show the relative frequencies for the fundamental (diamond), 1H (\times), and 2H (square) modes.

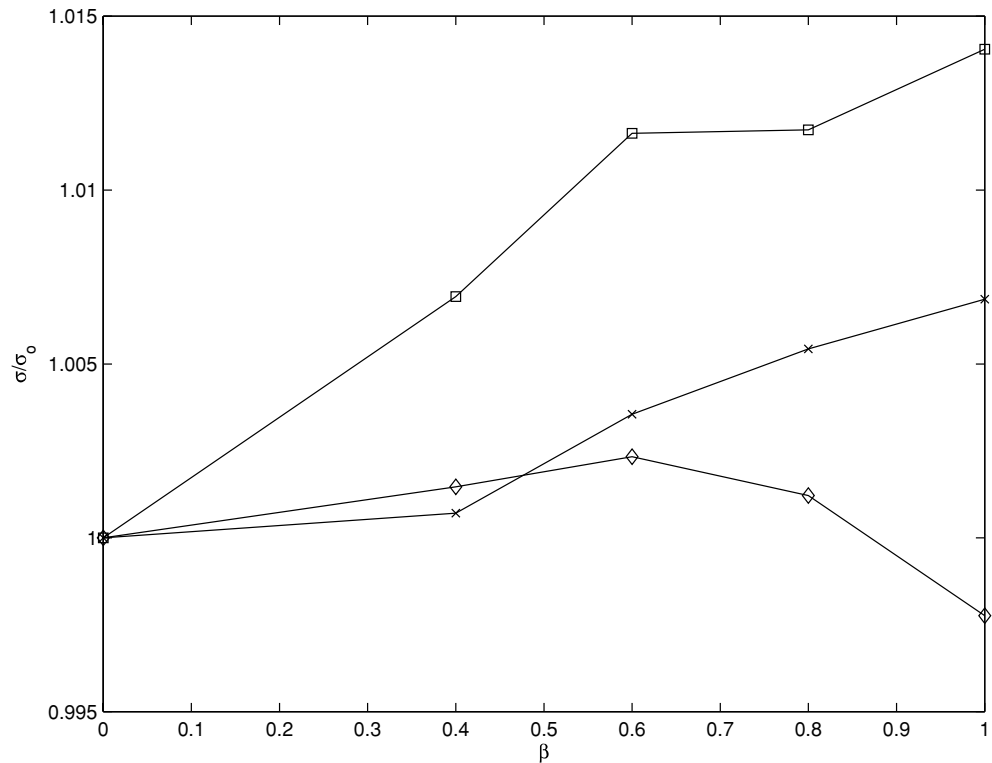


Figure 8. Relative frequencies of the $l_o = 1$ modes versus differential rotation parameter for a model rotating at 240 km s^{-1} . Shown are the p_1 (diamond), p_2 (\times), and p_3 (square) modes.

4. LARGE SEPARATIONS

If one considers two stellar models that are in the same evolutionary phase, and appear reasonably close to each other in the HR diagram, the frequencies can be approximately

determined from the relevant pulsation constant, Q . As the mass and radius change with position in the HR diagram, so will the frequencies. It is expected that for small changes in mass and radius the frequency differences (either frequency separations or ratios) will change, like Q , much more slowly than the individual

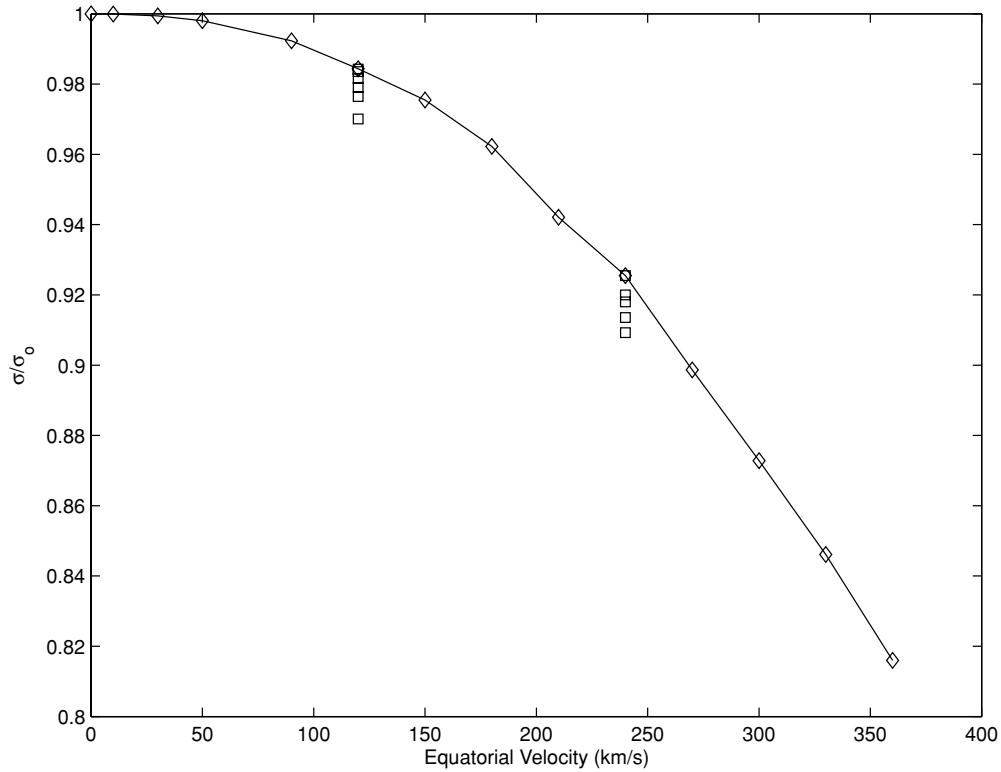


Figure 9. Relative effects of differential rotation for the $l_0 = 2 p_2$ mode. The frequencies for differentially rotating models as a function of β at 120 km s^{-1} and 240 km s^{-1} (squares) are superimposed on the uniformly rotating frequencies (diamonds).

frequencies. As a result, the large and small separations are probably more useful than individual frequencies as they are less sensitive to small changes in the models.

4.1. Uniform Rotation

The large separation, defined as

$$\Delta v_l = v_{l,n+1} - v_{l,n}, \quad (13)$$

can provide information about the outer layers of the stellar envelope. The large separation for the $l_o = 0$ mode is shown as a function of the rotation rate in Figure 10. We note that the overall trend of the large separation for this mode is to decrease as the rotation rate increases. At other l_o the trend is the same and the large separation decreases for every pair of modes considered. The magnitude of the decrease in large separation does increase slightly with increasing l_o , as can be seen by comparing Figures 10 and 11. For nonrotating ZAMS models, both the frequencies and the large separations decrease as the mass (hence the radius, luminosity, and effective temperature) increases. The decrease in the large separation occurs not only because the frequencies decrease, but also because the period ratios increase for increasing ZAMS mass. However, for stars observed approximately equator on, rotation decreases the perceived luminosity and effective temperature. This offset between the perceived luminosity and temperature and the large separation may be useful as a rotation discriminant. Of course, stars observed nearly pole on show an increase in perceived luminosity and effective temperature (e.g., Gillich et al. 2008) which is in line with the decreasing large separation as the rotation rate increases. Any discriminant of rotation may only be a matter of degree for low inclination objects.

We noted in Section 3.1 that the decrease in the frequencies with increasing rotation cannot be explained purely by the

decrease in the mean density (i.e., a constant Q). The mean density decreases faster than the pulsation periods increase as the rotation rate increases. Interestingly, the decrease in the large separation for $l_o = 0$ in Figure 10 is almost entirely offset by the mean density so that $\Delta v(\rho_\odot/\rho)^{1/2}$ is nearly constant, as discussed by Ulrich (1986) and Reese et al. (2008). The mean density does not offset the steeper decline in the large separation for the $l_o = 2$ modes shown in Figure 11.

4.2. Differential Rotation

The large separations provide information about the region near the surface of the star, while the frequencies provide information on more global properties. As discussed above, the separations are less sensitive to small changes in the mass or radius of the star but, since they probe the surface region, may provide information about changes in this region as a result of rotation. A comparison of Figures 2 and 3 shows that the polar radius is significantly more affected by differential rotation than the radius at lower latitudes. This kind of effect may be detectable using the large separations. Indeed, based on the results in the previous section, we expect there to be significant changes in the period differences as we have found that differential rotation can sometimes introduce a significant shift in only one or two of the harmonics.

Although the individual frequencies can show significant relative differences, this does not carry over to the large separations. The large separations for the $l_o = 0$ modes of a differentially rotating model with surface equatorial velocity of 120 km s^{-1} are shown in Figure 12. The large separations shown in this plot show very little change with increasing β , much less than the differences shown in Figure 10. The same lack of variation is seen for all modes. Given that the large separation probes the surface regions, this might be

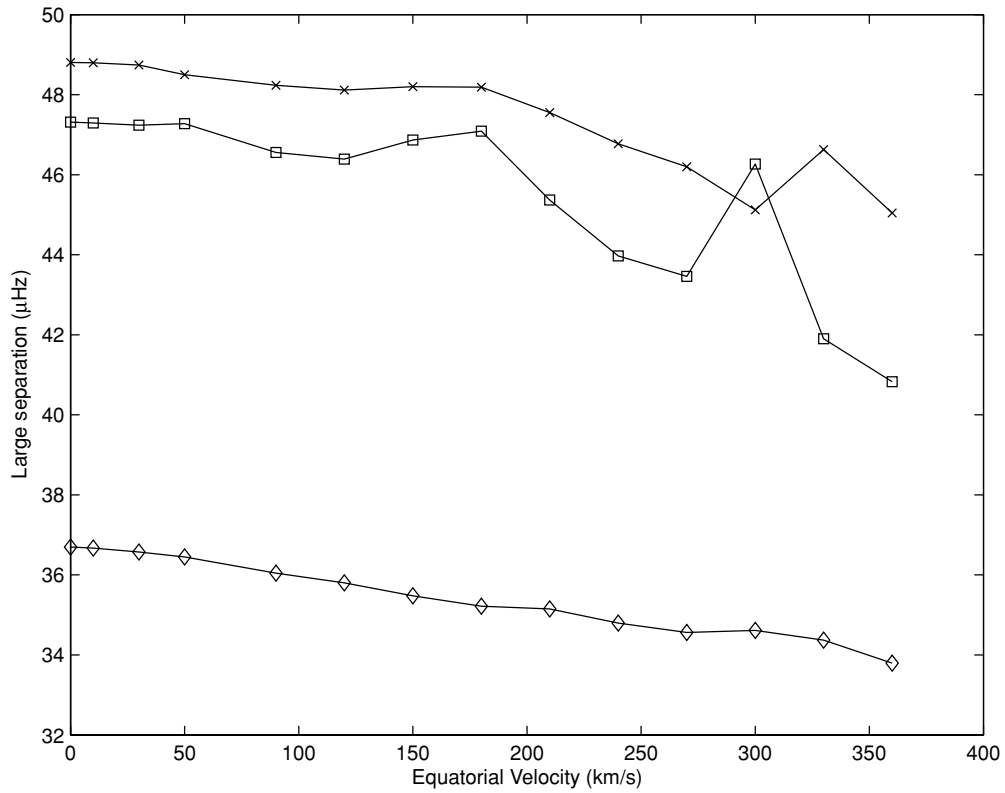


Figure 10. Large separation between the 3H and 2H (square), the 2H and 1H (×), and 1H and F modes (diamonds) for modes with $l_o = 0$.

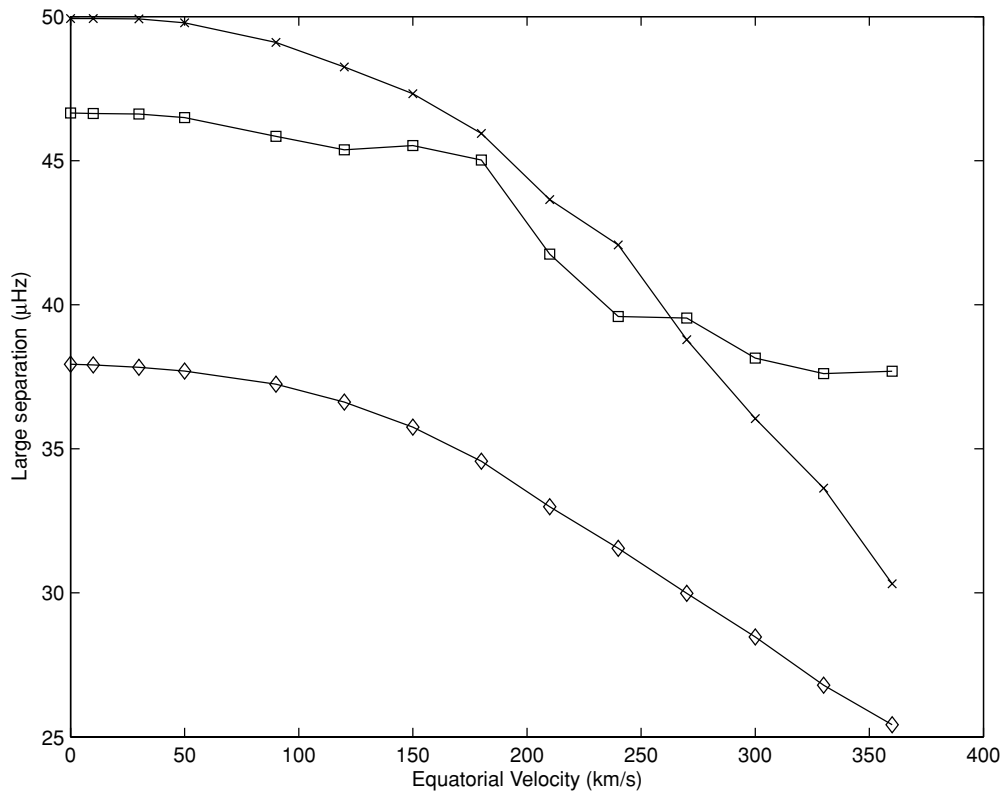


Figure 11. Large separation for the $l_o = 2$ modes as a function of rotation velocity. Shown are the separations between the p_1 and f modes (diamonds), the p_2 and p_1 modes (×), and the p_3 and p_2 modes (squares).

regarded as somewhat surprising because changing the β does change the surface configuration, particularly near the rotation axis.

At 240 km s^{-1} , the large separations shown in Figure 13 are again quite constant over the region shown. Most separations either remain constant or show a slight increase, at least to

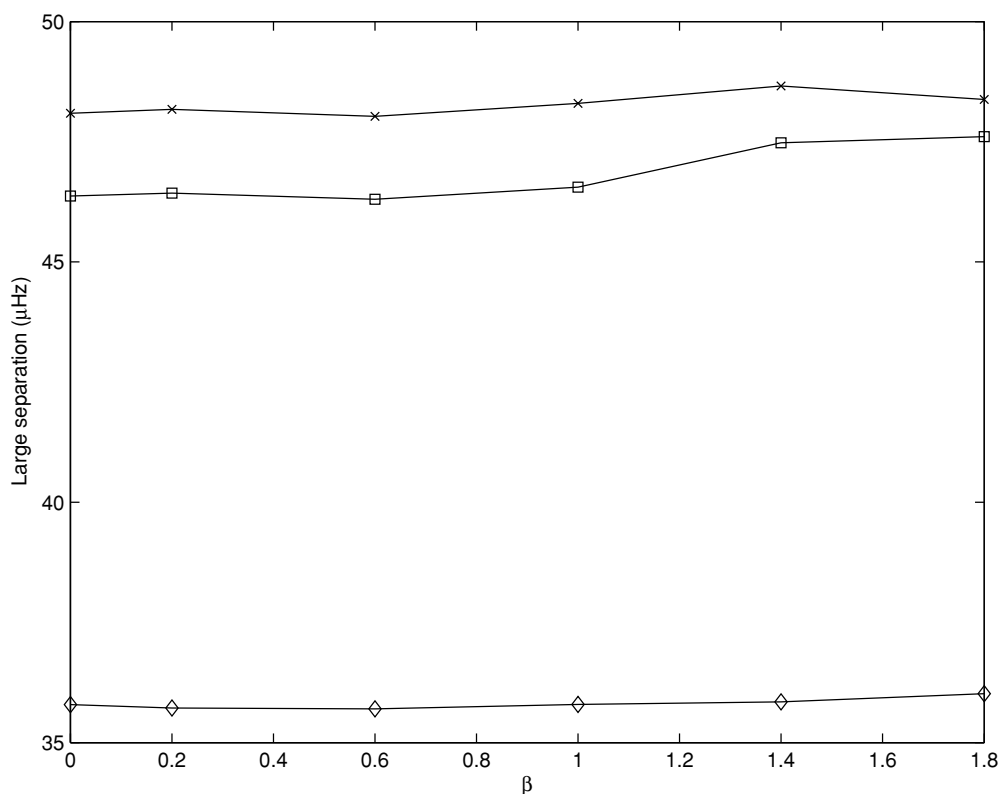


Figure 12. The large separation for the $l_o = 0$ modes of a differentially rotating model with a surface equatorial velocity of 120 km s^{-1} plotted as a function of differential rotation parameter β . Symbols are the same as Figure 10.

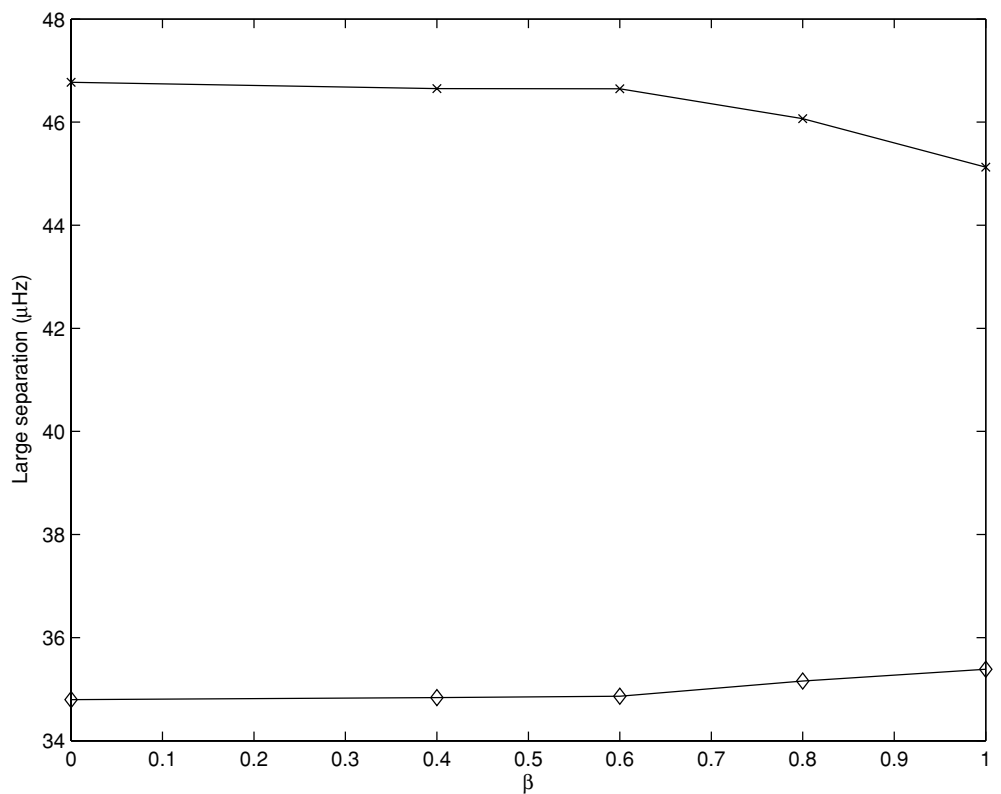


Figure 13. The large separation of the $l_o = 0$ modes for a differentially rotating model with a surface equatorial velocity of 240 km s^{-1} . Symbols are the same as in Figure 10.

$\beta = 0.6$, at which point some of the higher-order separations decrease slightly. Again, this is different from the trend seen

in the uniformly rotating models. Particularly at high β , the separations moving in different directions may allow constraints

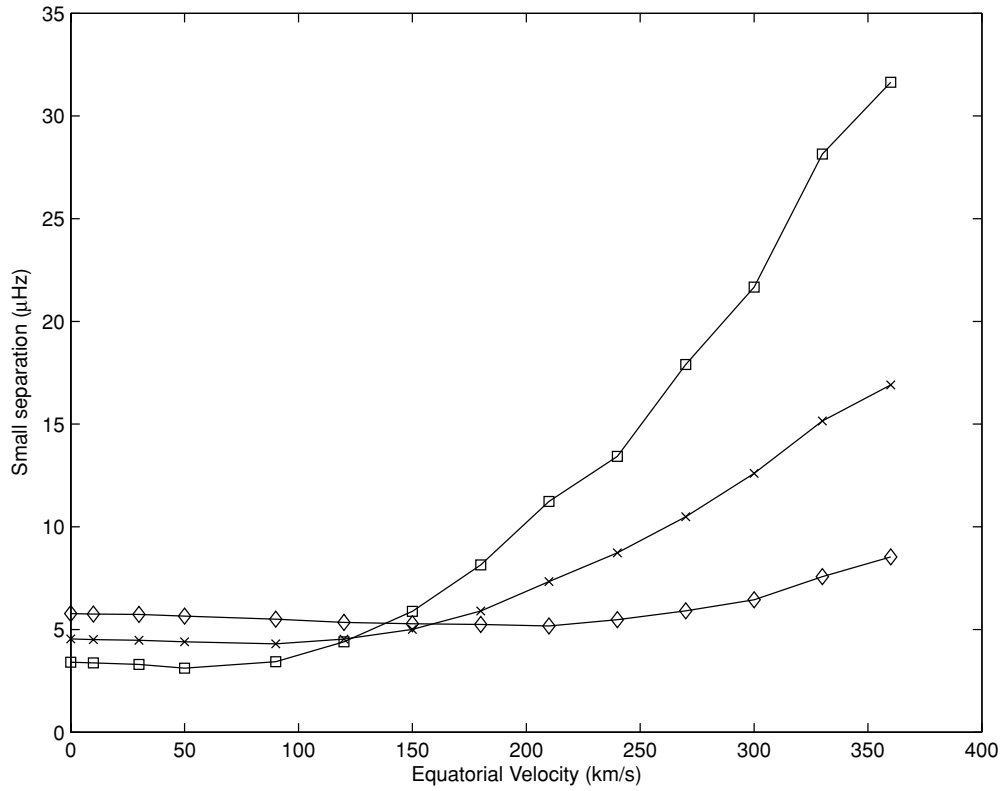


Figure 14. Small separation for the $l_o = 0$ and 2 modes as a function of surface equatorial velocity. Shown are the separations between the $l_o = 0, 3H - l_o = 2, p_2$ modes (squares), $l_o = 0, 2H - l_o = 2, p_1$ modes (\times), and $l_o = 0, 1H - l_o = 2, f$ modes (diamonds).

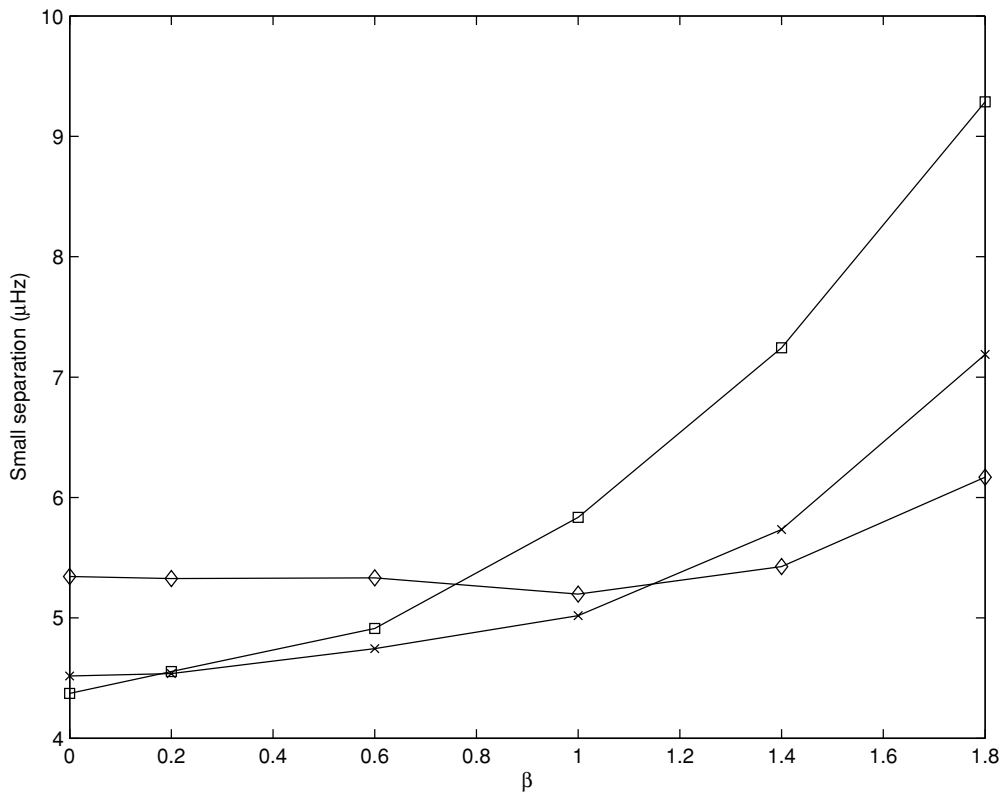


Figure 15. Small separations for the even modes for a differentially rotating model with a surface equatorial velocity of 120 km s^{-1} plotted as a function of differential rotation parameter β . Symbols are defined as in Figure 14.

to be placed on observed stars. The differences begin to become noticeable at $\beta \approx 0.6$ for most of the high-order modes

considered. However, for most modes the large separation never differs by more than a few μHz . As for the frequencies, it seems

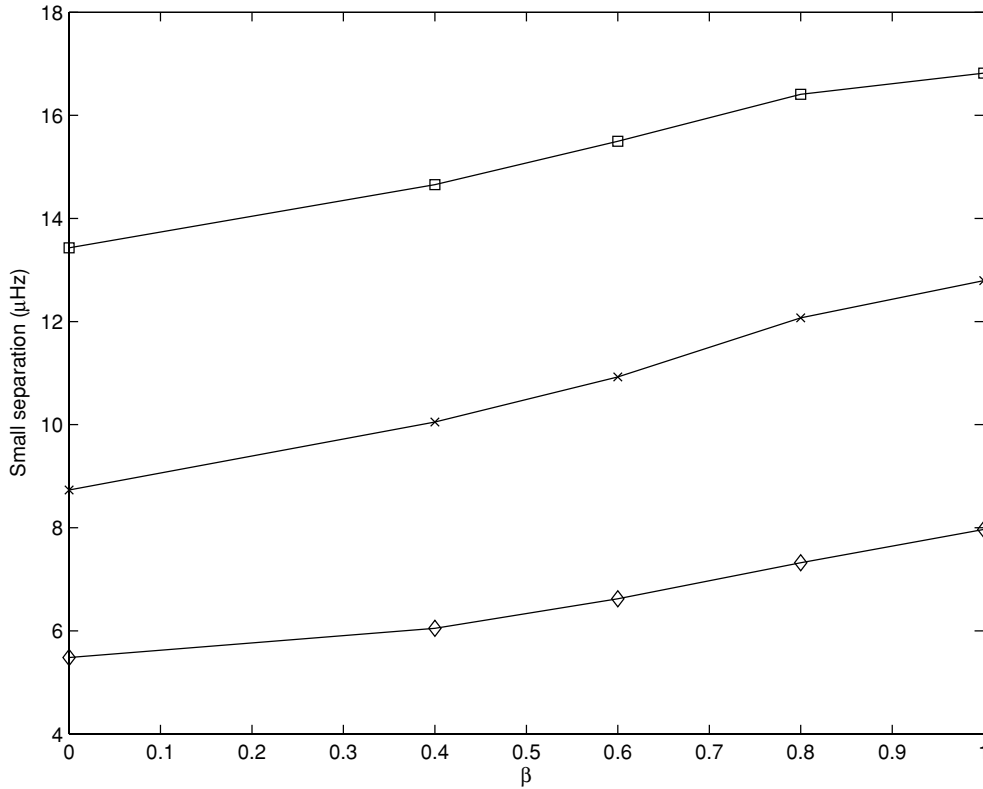


Figure 16. Small separations for the even modes of a differentially rotating model with a surface equatorial velocity of 240 km s^{-1} . Symbols are defined as in Figure 14.

that the large separations are unlikely to produce any very refined constraints on the internal rotation rate, at least for this particular rotation law.

5. SMALL SEPARATION

Asymptotic theory (Tassoul 1980), which predicts that the large separation should be approximately constant as n gets large, also predicts near degeneracy between modes with the same value of $n + l/2$:

$$v_{l,n} \simeq v_{l+2,n-1}. \tag{14}$$

The deviations from this degeneracy are defined as the small separation,

$$d_{l,n} = v_{l,n} - v_{l+2,n-1} \simeq -(4l + 6) \frac{\Delta v}{4\pi^2 v_{l,n}} \int_0^R \frac{dc}{dr} \frac{dr}{r}, \tag{15}$$

where c is the sound speed. The sound speed changes in the core are sufficiently large that the $(1/r)$ variation dominates the integral on the right-hand side of Equation (15), and hence the small separation is dominated by the structure in the core.

5.1. Uniform Rotation

At slow uniform rotation, the size and shape of the convective core are nearly unaltered by the rotation, and one would expect the effects on the small separation to be minimal. Figure 14 shows this to be true, but also shows that the small separation for higher n increases markedly with the rotation rate once the rotation exceeds approximately 150 km s^{-1} . There are slight changes to both the shape and relative size of the convective core with rotation, although the absolute mass and radius of the core change only slightly. It is not obvious why the small

separation increases so markedly. This effect has also been noted by Lignières et al. (2006)

Small separations are frequently used as probes of the core structure of stars, and can be used to constrain overshooting and core composition (Soriano & Vauclair 2008). Their results indicate that convective core overshooting causes a slight decrease in the small separations, with the effect becoming more pronounced as the star evolves. This slight trend is opposite to that produced by at least moderate rotation, which appreciably increases the small separation. Clearly this is a situation in which caution must be exercised when using observed modes to constrain conditions deep in the stellar interior.

5.2. Differential Rotation

For differentially rotating models, the overall trend is the same, with small separations increasing with increasing differential rotation. However, Figures 15 and 16 show that the variation in small separation is much less than for uniformly rotating models. The trends are consistent with the relationship between the effects of β and those of increasing the uniform rotation rate, as shown in Figure 9. The effects of increasing β on the convective core mimic to some extent those of increasing the uniform rotation rate, although high values of β do make the convective core more oblate. The different effects of β on the large and small separations is understandable in that increasing β increases the rotation and its effects near the rotation axis, and this certainly includes the convective core. However, this trend of increasing β producing similar trends to increasing uniform rotation rate does not give us confidence that we have a useful tool for diagnosing a rotation law of the kind we have considered through the small separation.

6. CONCLUSION

We have investigated the effects of uniform and differential rotation on pulsational eigenfrequencies. For uniformly rotating models, we have found that the frequencies decrease as the rotation rate increases for all values of l_o and n considered here, although the rate of decrease varies with the mode in question. While this frequency behavior is expected assuming the period–mean density relation applies, the frequency changes are much smaller than the period–mean density relation would suggest. We do find a pulsation constant being approximately constant if we use the surface radius at a colatitude of about 40° in the period–mean density relation, although this radius does not represent the mean density.

For the differential rotation law considered here, we find the frequencies at a given velocity may either increase or decrease, depending on l_o , with increasing differential rotation, relative to the uniformly rotating model. However, the overall effects in all cases are comparatively small, with maximum differences typically on the order of 1% when compared to the uniformly rotating case.

Uniform rotation decreases the large separation by several μHz ($< 10 \mu\text{Hz}$) over the entire range of rotation ($0\text{--}360 \text{ km s}^{-1}$) considered here. The large separation was virtually unchanged ($< 1 \mu\text{Hz}$) from that of uniform rotation for the range of differential rotation parameters considered here, despite the noticeable change in the surface shape. Although this change in shape is noticeable, it is still considerably smaller than the change produced by uniform rotation. Both uniform and differential rotation increase the small separation. The small separation can change markedly over the range of uniform rotation considered, while the dependence of the small separation on the rotation profile is more modest but not inconsistent with the other effects produced when comparing uniform and differential rotation. The effects of rotation on the frequencies and separations are generally large enough that rotation must be considered in the asteroseismology of these upper main-sequence stars. While the precise rotation rate at which one must be concerned with rotation depends on the level of accuracy achievable, it is certainly no larger than 100 km s^{-1} for our $10 M_\odot$ ZAMS models.

Although we have shown there can be significant differences in the pulsation properties of rotating stars, it is not clear that these results can actually be used to constrain the interior rotation rate. Given the possible combinations of effects from the rotation rate and distribution, the mass of the star, convective overshoot, evolutionary stage, etc., it seems unlikely that pulsation properties will give a unique solution, particularly if the number of observed modes is modest or cannot be properly identified. However, we have found that some combinations of modes constrain some of these properties.

This research was supported by the National Science and Engineering Research Council of Canada through a Discovery grant and a graduate fellowship. Computational facilities were provided with grants from the Canadian Foundation for Innovation and the Nova Scotia Innovation Research Trust.

REFERENCES

- Antia, H. M., & Basu, S. 2006, *ApJ*, **644**, 1292
 Baglin, A., Auvergne, M., Catala, C., & Michel, E., *The COROT Team 1998. ESA Spec. Publ.*, **464**, 395
 Basri, G., Borucki, W. J., & Koch, D. 2005, *New Astron. Rev.*, **49**, 478
 Basu, S., & Antia, H. M. 2004, *ApJ*, **606**, L85
 Belmonte, J. A., et al. 1993, in ASP Conf. Ser. 40, *Inside the Stars*, IAU Colloq. 137, ed. W. W. Weiss & A. Baglin (San Francisco, CA: ASP), 739
 Carcofi, A. C., Domiciano de Souza, A., Magalhães, A. M., Bjorkman, J. E., & Vakili, F. 2008, *ApJ*, **676**, L41
 Christensen-Dalsgaard, J., Gough, D. O., & Thompson, M. J. 1989, *MNRAS*, **238**, 481
 Christensen-Dalsgaard, J., Gough, D. O., & Thompson, M. J. 1991, *ApJ*, **378**, 413
 Clement, M. J. 1974, *ApJ*, **194**, 709
 Clement, M. J. 1978, *ApJ*, **222**, 967
 Clement, M. J. 1979, *ApJ*, **230**, 230
 Clement, M. J. 1998, *ApJS*, **116**, 57
 Couvidat, S., García, R. A., Turck-Chièze, S., Corbard, T., Henney, C. J., & Jiménez-Reyes, S. 2003, *ApJ*, **597**, L77
 Deupree, R. G. 1990, *ApJ*, **439**, 357
 Deupree, R. G. 1995, *ApJ*, **357**, 175
 Domiciano de Souza, A., Kervella, P., Jankov, S., Abe, L., Vakili, F., di Folco, E., & Paresce, F. 2003, *A&A*, **407**, L47
 Eff-Darwich, A., Korzennik, S. G., & Jiménez-Reye, S. J. 2002, *ApJ*, **573**, 857
 Gillich, A., Deupree, R. G., Lovekin, C. C., Short, I., & Toque, N. 2008, *ApJ*, **683**, 441
 Hacking, P., et al. 1999, in ASP Conf. Ser. 177, *Astrophysics with Infrared Surveys: A Prelude to SIRTf*, ed. M. D. Bica, R. M. Cutri, & B. F. Madore (San Francisco, CA: ASP), 409
 Iglesias, C. A., & Rogers, F. J. 1996, *ApJ*, **464**, 943
 Jackson, S., MacGregor, K. B., & Skumanich, A. 2005, *ApJS*, **156**, 245
 Lignières, F., Rieutord, M., & Reese, D. 2006, *A&A*, **455**, 607
 Lovekin, C. C., & Deupree, R. G. 2008, *ApJ*, **679**, 1499
 Nather, R. E., Winget, D. E., Clemens, J. C., Hansen, C. J., & Hine, B. P. 1990, *ApJ*, **361**, 309
 Ostriker, J. P., & Mark, J. W.-K. 1968, *ApJ*, **151**, 1075
 Reese, D., Lignières, F., & Rieutord, M. 2008, *A&A*, **481**, 449
 Rogers, F. J., Swenson, F. J., & Iglesias, C. A. 1996, *ApJ*, **456**, 902
 Sackmann, I.-J., & Anand, S. P. S. 1970, *ApJ*, **162**, 105
 Saio, H. 1981, *ApJ*, **244**, 299
 Schou, J., et al. 1998, *ApJ*, **505**, 390
 Smith, R. C. 1971, *MNRAS*, **151**, 463
 Soriano, M., & Vauclair, S. 2008, *A&A*, **488**, 975
 Stoeckley, T. R. 1968, *MNRAS*, **140**, 121
 Tassoul, M. 1980, *ApJS*, **43**, 469
 Tassoul, J. L. 2000, *Stellar Rotation* (Cambridge: Cambridge Univ. Press)
 Thompson, M. J., Christensen-Dalsgaard, J., Miesch, M. S., & Tommre, J. 2003, *ARA&A*, **41**, 599
 Ulrich, R. K. 1986, *ApJ*, **306**, L37
 Walker, G., et al. 2003, *PASP*, **115**, 1023
 Zahn, J.-P. 1992, *A&A*, **265**, 115